DMD Fast Forward. Published on January 25, 2019 as DOI: 10.1124/dmd.118.083279
This article has not been copyedited and formatted. The final version may differ from this version.

DMD # 83279

In vitro-In vivo extrapolation of key transporter activity at the blood-brain barrier

Patrick E. Trapa, Matthew D. Troutman, Thomas Y. Lau, Travis Wager, Tristan S. Maurer, Nandini C. Patel, Mark A. West, John P. Umland, Anthony Carlo, Bo Feng, Jennifer L. Liras

Pfizer Worldwide Research & Development, Pharmacokinetics, Dynamics & Metabolism (PDM), 1 Portland Street, Cambridge MA 02139 (P.E.T, T.S.M., J.L.L.); Pfizer Worldwide Research & Development, Pharmacokinetics, Dynamics & Metabolism (PDM), Groton, CT 06340 (M.T., M.A.W., J.P.U., A.C., B.F.); Pfizer Biomedicine Design, (T.Y.L.); Pfizer Medicinal Chemistry, 1 Portland Street, Cambridge MA 02139 (T.W., N.C.P)

DMD # 83279

Running Title: Blood-Brain Barrier IVIVE

Address correspondence to:

Jennifer L. Liras
1 Portland St.
Pfizer, Inc
Cambridge, MA 02139
Tel. 860 389-7938
Email: jennifer.liras@pfizer.com

Text pages: 25

Tables: 4 (+1 Supplemental Table)

Figures: 7

References: 24

Words in Abstract: 148

Words in Introduction: 655

Words in Discussion: 1163

Abbreviations:

BBB, blood-brain barrier; CNS, central nervous system; PBPK, Physiologically-based pharmacokinetic; IVIVE, *in vitro-in vivo* extrapolation; P-gp, P-glycoprotein; MDR1, multi-drug resistance protein 1; BCRP, Breast Cancer Resistance Protein; mBCRP, murine BCRP; UWL, unstirred water layer; MDCK, Madine-Darby Canine Kidney; ER, efflux ratio; DTT, dithiothreitol; IAA, iodoacetamide; SID, stable isotope dilution; SF, scaling factor; *REF*, relative expression factor; *RAF*, relative activity factor; $C_{b,u}$, unbound brain concentration; $C_{p,u}$, unbound plasma concentration $C_{b,u}/C_{p,u}$, steady-state unbound-brain to unbound-plasma concentration ratio; $f_{u,b\ \mathrm{cor}}$, corrected fraction unbound in brain: $f_{u,b}$, fraction unbound in brain; Acc_{lys}, lysosomal accumulation; V_{lys}, volume of lysosomal fraction; *pKa*, negative log of the acid dissociation constant; *pH,lys,* lysosomal pH; *pH,ECF,* extracellular pH; NHP, non-human primate; PK-PD, pharmacokinetic- pharmacodynamic; CSF, cerebrospinal fluid; AUC, area under the plasma curve

Abstract

Understanding the quantitative implications of P-gp and BCRP efflux is a key hurdle in the design of effective, centrally-acting or centrally restricted therapeutics. Previously, a comprehensive physiologically-based pharmacokinetic model was developed which describes *in vivo* unbound brain-to-plasma concentration ratio as a function of efflux activity measured *in vitro* (Trapa *et al*., 2016). In the present work, the predictive utility of this framework was examined through application to *in vitro* and *in vivo* data generated on 133 unique compounds across three preclinical species. Two approaches were examined for the scaling of efflux activity to *in vivo*, namely; relative expression as determined by independent proteomics measurements and relative activity as determined via fitting the *in vivo* neuropharmacokinetic data. The results with both approaches indicate that *in vitro* efflux data can be used to accurately predict the degree of brain penetration across species within the context of the proposed PBPK framework.

Introduction

Access of xenobiotics to the central nervous system is limited largely by the blood-brain barrier in microvessels of the brain (Abbott et al., 2010). The endothelial cells in these vessels are connected by tight junctions limiting paracellular penetration. They have reduced pinocytosis making passive permeability the major transcellular route of movement of lipophilic drugs into the brain. However the brain microvascular endothelium is also enriched with polarized transporters. Efflux transporters such as P-glycoprotein (P-gp; also commonly referred to as multi-drug resistance protein 1, MDR1) and breast cancer resistance protein (BCRP) efflux a diversity of passively permeable drug molecules back into the blood, while solute carrier proteins are thought to primarily bring polar nutrients into the brain.

Understanding these complex active and passive processes of movement into and out of the brain are critical to determining the rate and extent of drug penetration into the CNS and to the design of effective centrally-acting or safe centrally restricted therapeutics. Given its importance in the discovery and development of therapeutics intended to be active in the brain, the topic has been well reviewed (Mensch *et al*., 2009; Bicker *et al*., 2014; Stanimirovic *et al*, 2015). The concept of utilizing efflux transporters to restrict access to the CNS and avoid toxicity has also been reviewed (Bagal *et al*., 2014). To date most drug discovery optimization paradigms rely heavily on *in vitro* transporter assays and rodent neuropharmacokinetic evaluation which provide a qualitative assessment of human brain penetration (Di *et al*., 2013). A

quantitative prediction of clinical CNS drug penetration which integrates efflux from multiple transporters would be an enhancement to decision making.

Physiologically-based pharmacokinetic (PBPK) models simplify complex systems in order to describe them quantitatively. The resulting equations contain two types of parameters: those that characterize the biological system and those that capture aspects of the compound generally. The former inputs can be altered to enable translation across species, while the latter can describe a wide range of chemical matter. The ultimate utility of PBPK approaches, however, rests on one's ability to capture the physiology and parameterize the models accurately.

Parameterization can be accomplished by either relying on physiological scaling or fitting a large data set to extract the requisite scaling factors to support *in vitro – in vivo* extrapolation (IVIVE). Each method has its merits and pitfalls. Direct physiological scaling assumes that the model structure is perfect and that the data used to inform the model are both accurate and representative. These assumptions do not hold generally. For example, the permeability-surface area product at the blood-brain barrier might be estimated by multiplying *in vitro* permeability by the surface area of the vasculature. *In vitro* permeability can be limited by diffusion through an unstirred water layer (UWL) to the surface of the cells. In contrast, the UWL is vanishingly small *in vivo* owing to the convection of blood through relatively narrow microvasculature. The *in vitro* data therefore may not be reflective generally. When coupled with uncertainty around the precise surface area of the BBB, this disconnect can lead to poor model performance.

The second method can compensate for these shortcomings through estimating scaling factors; for example, by fitting a brain-uptake-index data set directly. The main caveats of such scaling center around how representative the underlying data are, and whether scaling is convolving together various sources of uncertainty (such as physiology, input parameter, and model structure). The fits are somewhat empirical rather than mechanistic which can lead to inaccuracy when extrapolating to species lacking data. Moreover, the scaling factors may lead to poor predictions for chemical matter that differs meaningfully from the training set.

The present work compares both approaches to scaling transporter activity at the BBB for BCRP and P-gp, two promiscuous active transporters that impact many current drugs, and drug-like chemical space. The caveats for each parameterization strategy are made explicit. In the end, both methods yield similar results lending confidence to the overall utility and robustness of the model.

Materials and Methods

Materials

Sprague-Dawley rat tissue (brain and plasma) were used in these binding studies and were obtained from Pel-Freez Biologicals (Rogers, AR). The MDR1-MDCK cells were obtained from the National Institutes of Health (Baltimore, MD). The mBCRP-MDCK cells were obtained from XenoPort (Santa Clara, CA). Test compounds utilized in these experiments were obtained from Pfizer global compound management or purchased from Sigma Aldrich (St. Louis, MO). Labware utilized for both permeability and equilibrium dialysis studies was per previous reports (Feng *et al*., 2008; Di *et al*., 2011a).

Methods

General well-established methods for permeability and binding assays were utilized consistently for all data presented in this work. A description of the general assay methods are described previously (Feng *et al*, 2008; Di et al, 2011b). Where appropriate, specific conditions are noted.

Cell culture for permeability assays: Permeability studies were conducted with murine BCRP-transfected MDCK cells (mBCRP-MDCK) and with MDR1-transfected MDCK cells (MDR-MDCK). Both cell lines were plated at 9.375E-5 cells / ml, and cultured for at least 4, but no longer than 5 days before use in experimentation. The mBCRP-MDCK cells utilize a tetracycline-inducible promoter, and therefore doxycycline was added to cell culture medium during seeding.

Permeability assay methods: *In vitro* assays were conducted utilizing well-established platform approaches for MDCK-based permeability assays (Feng *et al*., 2008; Di *et al*., 2011b). All experiments were performed with 2 μM test compound in transport buffer added to donor wells and measuring appearance in receiver wells after a 1.5 hour incubation at 37°C. For absorptive transport, the donor is the apical (A) compartment, and the receiver is the basolateral (B) compartment. For secretory transport, the donor is the B compartment, and the receiver is the A compartment.

Equilibrium Dialysis methods: Experiments to determine free and bound test compound were performed with rat brain homogenate and rat plasma per previously described methods (Kalvass *et al.*, 2002; Feng *et al*., 2008; Di *et al*., 2011a). Correlation studies have demonstrated a single species (e.g., Wistar Han rat) can be used as a predictor for brain tissue binding of any preclinical species or strain. Sample Analysis Methods: Samples from permeability and binding experiments were analyzed using high-throughput format liquid chromatography with tandem mass spectrometry using methods described by Kapinos and co-workers (Kapinos *et al*, 2017).

Data Analysis

Permeability Experiment Data Analysis: Determination of apparent permeability (P_{app}) and efflux ratio (ER) for all experiments utilized the following equations. The P_{app} was calculated using **equation 1**:

$$Papp = \frac{1}{Area\ X\ C_D(0)} \times \frac{dMr}{dt} \qquad Eq.1$$

Where area is the surface area of the cell monolayer (0.0625 cm^2), $C_D(0)$ is the initial concentration of test compound applied to the donor chamber, t is the time (in seconds), M_r is the mass of compound appearing in the receiver compartment as a function of time, and dM_r/dt is the flux of the compound across the cell monolayer. The ER was determined using **equation 2**:

$$ER = \frac{P_{app,BA}}{P_{app,AB}} \qquad Eq.2$$

Where AB and BA denote absorptive and secretory transport direction, respectively.

Binding experiment data analysis: The fraction unbound (f_u) was calculated using previously described equations (Kalvass *et al*., 2002; Feng *et al*., 2008; Di *et al*., 2011a) where brain homogenates were diluted 5-fold, and were corrected accordingly. Note that the brain free fraction was assumed to be equal across all species as this correlation has been previously demonstrated by Li Di and coworkers.

Proteomics. Targeted proteomics was used to measure MDR1 and BCRP in the cell lines used to generate the efflux ratios. Cell processing followed closely the methodology outlined by Uchida and coworkers (Uchida *et al*., 2011). Protein content was determined via stable isotope dilution multiple reaction monitoring mass spectrometry (SID-MRM) using a method adapted from Palandra and colleagues (Palandra *et al*, 2013). Briefly, cells were lysed in 8 M urea and protein concentrations determined by BCA assay. Cell lysates were then reduced with dithiothreitol (DTT) (10 mM 37°C for 30 min), alkylated with ioadoacetamide (IAA) (20 mM 37°C for 30 min in dark) and then enzymatically digested with trypsin. Quantification was enabled by

spiking in SID peptides corresponding to MDR1 (LANDAAQVK, NTTGALTTR) and BCRP1 (SSLLDVLAAR, VIQELGLDK) proteotypic peptides. SID peptides were labeled with C13N15 Arginine or Lysine C-terminii. Peptides were analyzed by LC-MS, specifically, loaded onto a C18 Pepmap trap and then subsequently separated by nanoflow on a C18 column over a 30 minute gradient directly ionizing into an ABSciex 4000 QTRAP. The MS was set MRM acquisition and monitored and masses corresponding to the precursors and 5 highest signal product ions. Resulting spectra were analyzed in Skyline software and quantification achieved by ratio of spiked "heavy" (20 fmol) with unknown endogenous "light."

Neuropharmacokinetic Studies

In vivo experiments were performed in accordance with the *Guide for the Care and Use of Laboratory Animals* (Institute of Laboratory Animal Resources, 1996) using protocols reviewed and approved by the WRD Institutional Animal Care and Use Committee (Groton, CT). As the neuropharmacokinetic data were derived from across multiple discovery projects with varied study designs, a general description of the methods is provided. Animal were dosed orally, subcutaneously or intraperitoneally to attain near pharmacologically relevant exposures. Whole blood samples were collected at time points appropriate to the pharmacokinetics in the species. The collection of whole blood from animals was achieved while under CO_2 (rat and mouse), isofluorane (rat, NHP) or following ketamine (NHP) anesthesia. Whole blood samples were drawn from either the jugular vein (rat) or direct cardiac puncture (mouse, rat, NHP) and stored on wet ice prior to centrifugation for harvest of serum sera or plasma. Brain tissue samples from mouse and rat (whole brain) and NHP (~1 g sections) were rinsed in saline, and

immediately frozen on dry ice. All samples were stored at -20 °C or -80 °C while pending bioanalytical analysis. Standard study and bioanalytical (LC-MS/MS) protocols have been previously published.(Doran *et al.*, 2012). Steady-state ratios of brain to plasma were calculated using the AUC method as described elsewhere.(Doran *et al*., 2012)

Modeling

Equation 3 estimates the steady-state unbound-brain/unbound-plasma ($C_{b,u}/C_{p,u}$) ratio from *in vitro* efflux ratios (ER) using corresponding scaling factors (SF) to account for expression and/or activity of Pgp and BCRP between *in vitro* and *in vivo* systems. Derivation of this equation is discussed elsewhere (Trapa *et al*., 2016), as it arises from a mechanistic model of brain penetration when several assumptions are made. The major assumptions are that the drug penetration is at steady state, active transport is governed only by two efflux transporters (whose flux is measured *in vitro* as ER_1 and ER_2), drug flux from bulk flow is minimal *in vivo* and paracellular diffusion is absent *in vitro*. In this work, *in vitro-to-in vivo* scaling factors (SF_1 and SF_2) for Pgp and BCRP were estimated by two independent approaches. In the first approach, a relative expression factor (*REF*) was estimated via proteomics measurements in each system. In the second, a relative activity factor was estimated by fitting the observed unbound brain-to-unbound plasma data (**Supplemental Table 1)** using **equation 3** (NONMEM V, ICON). In the latter, the relationship of *REF* values between species was set with abundance data (Ito *et al*., 2011; Uchida *et al.*, 2011; Hoshi *et al*., 2013) (**Table 1**). As such, only one set of *RAF* values was estimated to support rather than determining scaling factors independently for each species.

DMD Fast Forward. Published on January 25, 2019 as DOI: 10.1124/dmd.118.083279
This article has not been copyedited and formatted. The final version may differ from this version.

$$\frac{C_{b,u}}{C_{p,u}} = \frac{1}{SF_1 \times (ER_1 - 1) + SF_2 \times (ER_2 - 1) + 1} \qquad Eq.3$$

As originally described, the determination of $C_{b,u}$ / $C_{p,u}$ ratio requires the estimation of total concentrations in plasma and brain via *in vivo* neuropharmacokinetic studies and the independent estimation on $f_{u,b}$ and $f_{u,p}$ via equilibrium dialysis (Kalvass *et al*., 2002). The estimation of f_{ub} requires the use of homogenized brain tissue and a calculation to account for the dilution of tissue required in the homogenization process. One limitation to this approach is that the $f_{u,b}$ measures obtained from tissue homogenate fail to capture drug accumulation that occurs *in vivo* via pH partitioning. Of particular concern is the potential for basic compounds to significantly partition into acidic lysosomal subcompartments, a phenomenon that has been mathematically addressed previously (Fridén *et al*., 2011). **Equations 4 and 5** can be used together to correct for potential lysosomal accumulation. **Equation 4** explicitly assumes that the experimental *in vitro* homogenate binding value ($f_{u,b}$) would apply in all subcellular compartments, but also accounts for pH partitioning to lysosomes to get an effective unbound fraction *in vivo* ($fu_{b,cor}$). For example, if lysosomal accumulation (Acc_{lys}) increases the overall cell concentration by 100% (i.e. Acc_{lys} = 1), the effective in *in vivo* fu_b ($fu_{b,cor}$) would be two-fold lower than that estimated via equilibrium dialysis (fu_b). In order to calculate Acc_{lys}, one needs to account for the anticipated pH partitioning and the fractional lysosomal volume of the cell.

Equation 5 assumes that the Henderson-Hasselbalch equation holds; the compounds are treated as monoprotic bases or neutrals. V_{lys} represents the volume lysosomal fraction, set at 1% for this analysis. *pKa*, *pH,lys* and *pH,ECF* are the basic compound

DMD Fast Forward. Published on January 25, 2019 as DOI: 10.1124/dmd.118.083279
This article has not been copyedited and formatted. The final version may differ from this version.

pKa, lysosomal pH, and extracellular pH, respectively. The latter two values are assumed to be 5.0 and 7.4, respectively. The pKa values for each compound were generated via the in silico MoKa approach (Milletti *et al*., 2007).

$$f_{u,b\ cor} = \frac{f_{u,b}}{1 + Acc_{lys}} \qquad Eq.4$$

$$Acc_{lys} = V_{lys} \times \frac{1 + 10^{(pKa - pH,lys)}}{1 + 10^{(pKa - pH,ECF)}} \qquad Eq.5$$

Results

Supplemental Table 1 lists the attributes of the compounds. Overall, the set contains 64, 68, and 15 steady-state brain and plasma-concentration measurements for mouse, rat, and non-human primate (NHP), respectively. The distribution of efflux ratios and ratios of free brain to free plasma concentrations with and without brain-homogenate binding corrections are illustrated in **Figures 1 and 2.** The results span a wide range of brain restriction and efflux ratios, but basic and neutral compounds dominate the list**.** We chose to utilize the mBCRP cell line in these studies based on a number of factors. First, we have found that these cells show much better inter-experimental reproducibility and dynamic range versus the human BCRP line (in which endogenous dog MDR1 must be inhibited), providing comparable data across multiple experiments. Second, internal assessment of a large set of diverse, drug-like molecules demonstrated a strong correlation between efflux in mBCRP and human BCRP cells (R2 = 0.86; data not shown, manuscript in preparation).

DMD Fast Forward. Published on January 25, 2019 as DOI: 10.1124/dmd.118.083279
This article has not been copyedited and formatted. The final version may differ from this version.

Proteomics analysis of MDR1 and BCRP cells lines determined protein contents of 36 and 60 fmol/μg respectively. Scaling factors for the efflux ratios from both methods with and without lysosomal accumulation are captured in **Table 2. Figures 3 and 4** illustrate the corresponding observed and predicted $C_{b,u}/C_{p,u}$ for the *RAF* and *REF* approach to IVIVE, respectively. **Table 3** contains the corresponding percentages of $C_{b,u}/C_{p,u}$ fold error for predictions made with parameters estimated without the brain-binding correction and the cumulative distribution of fold error for each species (using *RAF* values) is depicted in **Figure 5**. **Figure 6** projects human brain penetration as a function of efflux using *RAF* values.

Discussion

Using the *REF* approach (**Table 1**), a good concordance was observed between predicted and observed $C_{b,u}/C_{p,u}$ across species (**Figure 4**). This concordance implies that the assumption that activity scales with abundance holds. While this may stand in contrast to other work suggesting there exists the potential for differences in activity between species orthologues (particularly in K_m)(Kato M, 2006), this translational result is consistent with the notion that inherent transport activity differences across species is negligible for this set of 133 compounds across the three species examined. The expression data therefore suggest that P-gp (MDR1) substrates will show an improvement in brain penetration in primates over rodents commensurate with this difference. Given this result, it is perhaps not surprising that model-based estimation of *RAF* values also provided a good characterization of the data (**Figure 3**) and yields trends across species that were consistent with the relative expression data (**Table 2**).

DMD Fast Forward. Published on January 25, 2019 as DOI: 10.1124/dmd.118.083279
This article has not been copyedited and formatted. The final version may differ from this version.

While both approaches to IVIVE produce models capable of rank-ordering compounds effectively, the *REF* (proteomics-based) approach without lysosomal-accumulation correction led to a systematic under prediction of the *in vivo* brain penetration (**Figure 4**, $C_{b,u}/C_{p,u}$ plots). Notably, the ratio of the MDR1 and BCRP scaling factors is still similar between the forward and fit method without lysosomal correction (**Table 2**). However, the magnitudes differ. One of the challenges of the *REF* approach is normalizing the measured protein concentrations appropriately across various samples and tissues. In the case of proteomics analysis, disparities in the extraction of the proteins *in vitro* and *in vivo* might explain part of the discrepancy in scaling factors. However, when accounting for pH-partitioning in brain binding, the *RAF* estimates fall into very close agreement (**Table 2**). Likewise, the *REF* method provided an improved prediction of *in vivo* brain penetration after accounting for pH partitioning (**Figure 4**, $C_{b,u}/C_{p,u}$,($f_{u,b,cor}$) plots). Though mechanistically accurate, correcting brain-binding measurements for lysosomal accumulation does not yield improvement in fit quality for the *RAF* approach (**Table 3**); however, the use of $f_{u,b,\mathrm{cor}}$ does reduce the number of compounds with observed $C_{b,u}/C_{p,u} > 1$ (**Figure 2**). This is an important finding in that it lends support for the *REF* based approach which might otherwise be considered inadequate. In addition, for the compounds with $C_{b,u}/C_{p,u} > 1$, it provides a straight-forward explanation for what might otherwise be interpreted as the presence of an active uptake process. These findings are entirely consistent with previous work and provide further support for systematic accounting of lysosomal partitioning in such analyses (Fridén *et al.*, 2011). The method requires an accurate pKa determination; $f_{u,b,\mathrm{cor}}$ therefore could change as measured pKa values are substituted for model predictions. The correction also

renders comparison to historical data challenging. Pragmatically, efficacy is also estimated via the *in vivo* free-brain concentrations, so inaccuracy in free concentrations as a result of $f_{u,b}$ measures would be compensated by the pharmacokinetic-pharmacodynamics (PK-PD) parameters obtained preclinically. In light of these practical considerations, the authors implemented the fitted scaling factors without binding correction to support internal decision making. Using this parameterization, the implications of *in vitro* ER ratios for *in vivo* $C_{b,u}/C_{p,u}$ can be readily determined. (**Figure 6**).

Figure 7 illustrates the overall comprehensive strategy for brain-penetration prediction. Machine-learning computational ADME models are capable of producing high quality predictions of efflux ratios for virtual compounds thereby affording the opportunity to enrich libraries prior to synthesis. *In vitro*, all assays are well characterized statistically. Real-time statistical tools allow for quality control as well as for optimization of replication strategies to meet the data-quality and cycle-time needs of specific project teams. Predictions are made via efflux ratios, but additional *in vivo* data continue to be generated opportunistically. Comparison between the prospective prediction and *in vivo* results serves as a check of the IVIVE. Finally, all data are captured allowing for continuous refinement of the models which includes machine learning as well as the scaling described presently.

The approach has proved effective over several years for guiding optimization and selection of CNS clinical candidates, but several key caveats remain:

1. The analysis only holds for permeable bases and neutrals. The model structure incorporates only BCRP and MDR1 (P-gp). While the literature is limited, acids are purportedly restricted via other transporters.(Mori S, 2003; Leggas M, 2004) Moreover in this model, flux into the brain is assumed to dominate over bulk flow. As such, this method may be misleading when applied to poorly permeable molecules and those that are anionic or zwitterionic in nature.

2. Generally, scaling with proteomics alone must be normalized appropriately across tissues and cell lines, particularly when extraction may vary. Activity is explicitly assumed to scale with abundance, which may not be the case for all transporters.

3. Suitable parameter estimation requires a large and diverse data set. For example, rodent data alone would not lead to high confidence in the *RAF* values. Compounds are either dual substrates or P-gp-specific substrates (**Supplemental Table 1, Figure 1**), and P-gp expression is much greater than BCRP in rodents (**Table 1**); detecting the BCRP component therefore is difficult. Even relatively sparse NHP data help constrain the solution space allowing for unique parameter estimation.

4. The accuracy depends greatly on the quality of input parameters and data. Predictions using **Equation 3** require ER values for each efflux transporter, both containing two individual experiments and attendant variability associated with these studies. The observed $C_{b,u}/C_{p,u}$ contains four measures as well: $f_{u,p}$, $f_{u,b}$ along with total brain and plasma concentrations. Any of these eight experimental values can lead to discordance in the IVIVE.

5. The framework is assay dependent. ER values for control compounds are listed in **Table 4** so that researchers might calibrate assay results in order to gain value from the model.

Given the caveats above, the present model does not completely obviate the need for *in vivo* experiments to understand brain penetration. These data can be generated opportunistically as part of a pharmacology study in lower-order species or as an endpoint in toxicology studies for higher-order species. *In vivo* data afford a means to confirm $C_{b,u}/C_{p,u}$ and provide valuable information regarding *in vitro-in vivo* correlation. Deviations between the observed and predicted value may be due to variability, or may serve as an alert that the model structure is insufficient (i.e. excludes aspects such as uptake or additional efflux transporters).

Future directions could include expanding the transporters to include those responsible for efflux beyond P-gp and BCRP or uptake. With regard to efflux transporters, it is likely that BCRP and P-gp account for majority of transporter-mediated restriction at the blood brain barrier. However, there are reports of additional transporters impacting brain efflux and uptake (Kanamitsu *et al*., 2017; Sano *et al*., 2018) Efforts to characterize mechanistically the relationship between cerebrospinal fluid (CSF) and free-brain concentrations would also be useful. Such a relationship would provide a second measure in terminal studies to account for variability in input parameters, a non-terminal method to estimate brain penetration in higher order species, and confidence in utilizing CSF data in humans to project brain concentrations.

Declaration of conflicts of interest

The authors hereby declare no conflicts of interest.

Authorship Contributions

Participated in research design: Patrick Trapa, Jennifer Liras, Matt Troutman, Bo Feng, Travis Wager, Tristan S. Maurer

Conducted experiments: Thomas Y. Lau, John P. Umland, Mark A. West

Contributed new reagents or analytic tools: Bo Feng, Anthony Carlo

Performed data analysis: Patrick E. Trapa, Thomas Y. Lau, Nandini C. Patel

Wrote or contributed to the writing of the manuscript: Patrick E. Trapa, Jennifer L. Liras, Thomas Lau, Matt Troutman, Tristan S. Maurer

References

Abbott NJ, Patabendige AAK, Dolman DEM, Yusof SR, Begley DJ (2010) Structure and function of the blood-brain barrier. *Neurobiology of Disease* **37:**13-25.

Bagal S, Bungay P (2014) Restricting CNS penetration of drugs to minimise adverse events: role of drug transporters. *Drug Discov Today: Technol* **12:**79-85.

Bicker J, Alves G, Fortuna A, Falcão A (2014) Blood–brain barrier models and their relevance for a successful development of CNS drug delivery systems: A review. *Eur J Pharm Biopharm* **87:**409–432.

Di L Rong H, Feng B (2013) Demystifying Brain Penetration in Central Nervous System Drug Discovery. *J Med Chem* **56:**2-12.

Di L, Umland JP, Chang G, Huang Y, Lin Z, Scott DO, Troutman MD, Liston TE (2011a) Species Independence in Brain Tissue Binding Using Brain Homogenates. *Drug Metab Dispos* **39:**1270–1277.

Di L, Whitney-Pickett C, Umland JP, Zhang H, Zhang X, Gebhard DF, Lai Y, Federico JJ, Davidson RE, Smith R, Reyner EL, Lee C, Feng B, Rotter C, Varma MV, Kempshall S, Fenner K, El-kattan AF, Liston, TE, Troutman MD (2011b) Development of a new permeability assay using low-efflux MDCKII cells. *J Pharm Sci* **100:**4974-4985.

Doran A, Osgood S, Mancuso J, Shaffer C (2012) An evaluation of using rat-derived single-dose neuropharmacokinetic parameters to project accurately large animal unbound brain drug concentrations. *Drug Metab Dispos* **40:**2162-2173.

Feng B, Mills JB, Davidson RE, Mireles RJ, Janiszewski JS, Troutman MD, de Morais SM (2008) In Vitro P-glycoprotein Assays to Predict the in Vivo Interactions of P-glycoprotein with Drugs in the Central Nervous System. *Drug Metab Dispos* **36:**268–275.

Fridén M, Bergström F, Wan H, Rehngren M, Ahlin G, Hammarlund-Udenaes M, Bredberg U. (2011) Measurement of unbound drug exposure in brain: modeling of pH partitioning explains diverging results between the brain slice and brain homogenate methods. *Drug Metab Dispos* **39:**353-362.

Hoshi Y, Uchida Y, Tachikawa M, Inoue T, Ohtsuki S, Terasaki T (2013) Quantitative Atlas of Blood–Brain Barrier Transporters, Receptors, and Tight Junction Proteins in Rats and Common Marmoset. *J Pharm Sci* **102:**3343-3355.

Ito K, Uchida Y, Ohtsuki S, Aizawa S, Kawakami H, Katsukura Y, Kamiie J, Terasaki T (2011) Quantitative membrane protein expression at the blood-brain barrier of adult and younger cynomolgus monkeys *J Pharm Sci* **100:**3939-3950.

Kalvass JC, Maurer TS (2002) Influence of nonspecific brain and plasma binding on CNS exposure: implications for rational drug discovery. *Biopharm Drug Dispos* **23:**327–338.

Kanamitsu K, Kusuhara H, Schuetz JD, Takeuchi K, Sugiyama Y (2017) Investigation of the importance of multidrug resistance associated protein 4 (Mrp4/Abcc4) in the active efflux of anionic drugs across the blood–brain barrier. *J Pharm Sci* **106:**2566–2575.

K Kapinos B, Liu J, Piotrowski M, Keefer J, Holder B, Janiszewski J, Zhang H, Troutman M (2017) Development of a high-performance, enterprise-level, multimode LC-MS/MS autosampler for drug discovery. *Bioanalysis* **9:**1643-1654.

Kato M, Suzuyama N, Takeuchi T, Yoshitomi S, Asahi S, Yokoi T (2006) Kinetic Analyses for Species Differences in P-glycoprotein-Mediated Drug Transport. *J Pharm Sci* **95:**2673-2683.

Leggas M, Adachi M, Scheffer GL, Sun D, Wielinga P, Du G, Mercer KE, Zhuang Y, Panetta JC, Johnston B, Scheper RJ, Stewart CF, Schuetz JD (2004) Mrp4 confers resistance to topotecan and protects the brain from chemotherapy. *Mol Cell Biol* **24:**7612-7621.

Mensch J, Oyarzabal J, Mackie C, Augustijns P, (2009) In vivo, in vitro and in silico methods for small molecule transfer across the BBB. *J Pharm Sci* **98:**4429-4468.

Milletti F, Storchi L, Sforna G, Cruciani G (2007) New and original pKa prediction method using grid molecular interaction fields. *J Chem Inf Model* **47:**2172-2181.

Mori S, Takanaga H, Ohtsuki S, Deguchi T, Kang Y-S, Hosoya K-i, Terasaki T (2003) Rat Organic Anion Transporter 3 (rOAT3) Is Responsible for Brain-to-Blood Efflux of Homovanillic Acid at the Abluminal Membrane of Brain Capillary Endothelial Cells. *J Cereb Blood Flow Metab* **23:**432–440.

Palandra J, Finelli A, Zhu M, Masferrer J, Neubert H (2013) Highly Specific and Sensitive Measurements of Human and Monkey Interleukin 21 Using Sequential Protein and Tryptic Peptide Immunoaffinity LC-MS/MS. *Anal Chem* **85:**5522−5529.

Sano Y, Mizuno T, Mochizuki T, Uchida Y, Umetsu M, Terasaki T, Kusuhara H (2018) Evaluation of Organic Anion Transporter 1A2-knockin Mice as a Model of Human Blood-Brain Barrier. *Drug Metab Dispos DOI: 10.1124/dmd.118.081877*.

Stanimirovic DB B-YM, Perkins M, Haqqani AS (2015) Blood-brain barrier models: in vitro to in vivo translation in preclinical development of CNS-targeting biotherapeutics. *Expert Opin Drug Disc* **10:**141-155.

Trapa PE, Belova E, Liras JL, Scott DO, and Steyn SJ (2016) Insights From an Integrated Physiologically Based Pharmacokinetic Model for Brain Penetration. *J Pharm Sci* **105:**965-971.

Uchida Y, Ohtsuki S, Katsukura Y, Ikeda C, Suzuki T, Kamiie J, Terasaki T (2011) Quantitative targeted absolute proteomics of human blood-brain barrier transporters and receptors. *J Neurochem* **117:**333-345.

DMD Fast Forward. Published on January 25, 2019 as DOI: 10.1124/dmd.118.083279
This article has not been copyedited and formatted. The final version may differ from this version.

Legend for Figures

Figure 1. Distribution of the ER values of the compounds in **Supplemental Table 1**.

Figure 2. Cumulative distribution of ratios of free-brain and free-plasma concentrations with or without pH-partitioning correction to the homogenate-derived brain binding values.

Figure 3. Observed and predicted ratios of free-brain and free-plasma concentrations with or without pH-partitioning correction to the homogenate-derived brain binding values using *RAF* values obtained from parameter estimation. The solid and dashed lines represent unity and two-fold error respectively.

Figure 4. Observed and predicted ratios of free-brain and free-plasma concentrations with or without pH-partitioning correction to the homogenate-derived brain binding values using *REF* values obtained using the ratios of protein expression from the cell lines to the tissues. The solid and dashed lines represent unity and two-fold error respectively.

Figure 5. Cumulative distribution of fold error for each species using *RAF* values derived from parameter estimation without brain-binding correction.

Figure 6. Forward estimation of the ratio of free-brain and free-plasma concentration in humans using the *RAF* values derived from parameter estimation without brain-binding correction.

Figure 7. Schematic of the overall implementation strategy for brain-penetration prediction. Continuous data capture allows for refinement of both *RAF* values and machine-learning models for *in vitro* data.

Tables

Table 1. Protein expression of MDR1 (P-gp) and BCRP across species.

	Mouse[(a)]	*Rat**[(b)]	*NHP*[(c)]	*Human*[(a)]
MDR1 (fmol/ug)	14.1	19.1	4.71	6.06
BCRP (fmol/ug)	4.41	4.95	14.2	8.14

* average of Wistar and Sprague Dawley (a) Uchida et al., 2011 (b) Hoshi et al., 2013 (c) Ito et al., 2011

Table 2. Proteomic Relative Expression (*REF*) and Parameter Estimate Relative Activity (*RAF*) factor estimations.

	MDR1				***BCRP***			
REF	**Mouse**	**Rat**	**NHP**	**human**	**mouse**	**Rat**	**NHP**	**Human**
Proteomics	0.39	0.53	0.13	0.17	0.074	0.083	0.237	0.136
RAF **Parameter estimate**	0.24	0.33	0.08	0.10	0.049	0.055	0.157	0.09
(SEM)	(0.07)	(0.09)	(0.02)	(0.03)	(0.024)	(0.027)	(0.077)	(0.044)
RAF **Parameter estimate, $f_{ub,\ cor}$**	0.36	0.491	0.12	0.16	0.049	0.055	0.157	0.090
(SEM)	(0.06)	(0.08)	(0.02)	(0.03)	(0.02)	(0.022)	(0.063)	(0.036)

Table 3. Percentage of predictions within two fold of observed for each of the scaling factor (proteomic *REF* and parameter estimate *RAF)* sets - with and without $f_{u,b}$ correction.

	Proteomics		**parameter estimate**	
	$f_{u,b}$	**$f_{u,b\ cor}$**	**$f_{u,b}$**	**$f_{u,b\ cor}$**
Mouse	72%	77%	66%	67%
Rat	65%	72%	76%	71%
NHP	93%	73%	87%	60%

Table 4. Efflux Ratio values for select control compounds.

	MDR1 ER	***mBCRP ER***
Prazosin	21.1	50.8
Quinidine	78.2	3.0
Triprolidine	3.3	2.2
Metroprolol	2.5	1.2
Fleroxacin	3.5	6.4
Pitavastatin	16.3	80.5

DMD Fast Forward. Published on January 25, 2019 as DOI: 10.1124/dmd.118.083279
This article has not been copyedited and formatted. The final version may differ from this version.

Figures

Figure 1.

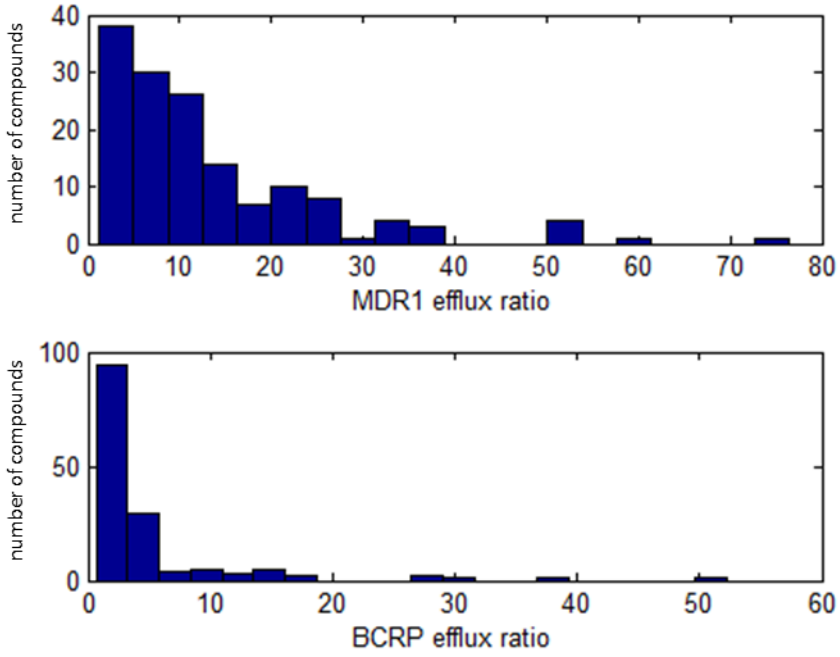

DMD Fast Forward. Published on January 25, 2019 as DOI: 10.1124/dmd.118.083279
This article has not been copyedited and formatted. The final version may differ from this version.

Figure 2.

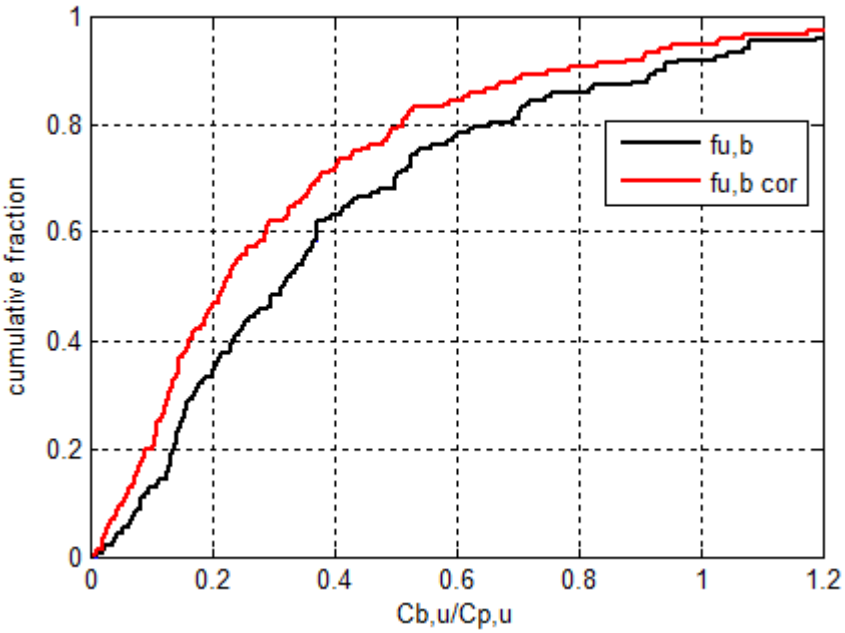

DMD Fast Forward. Published on January 25, 2019 as DOI: 10.1124/dmd.118.083279
This article has not been copyedited and formatted. The final version may differ from this version.

Figure 3.

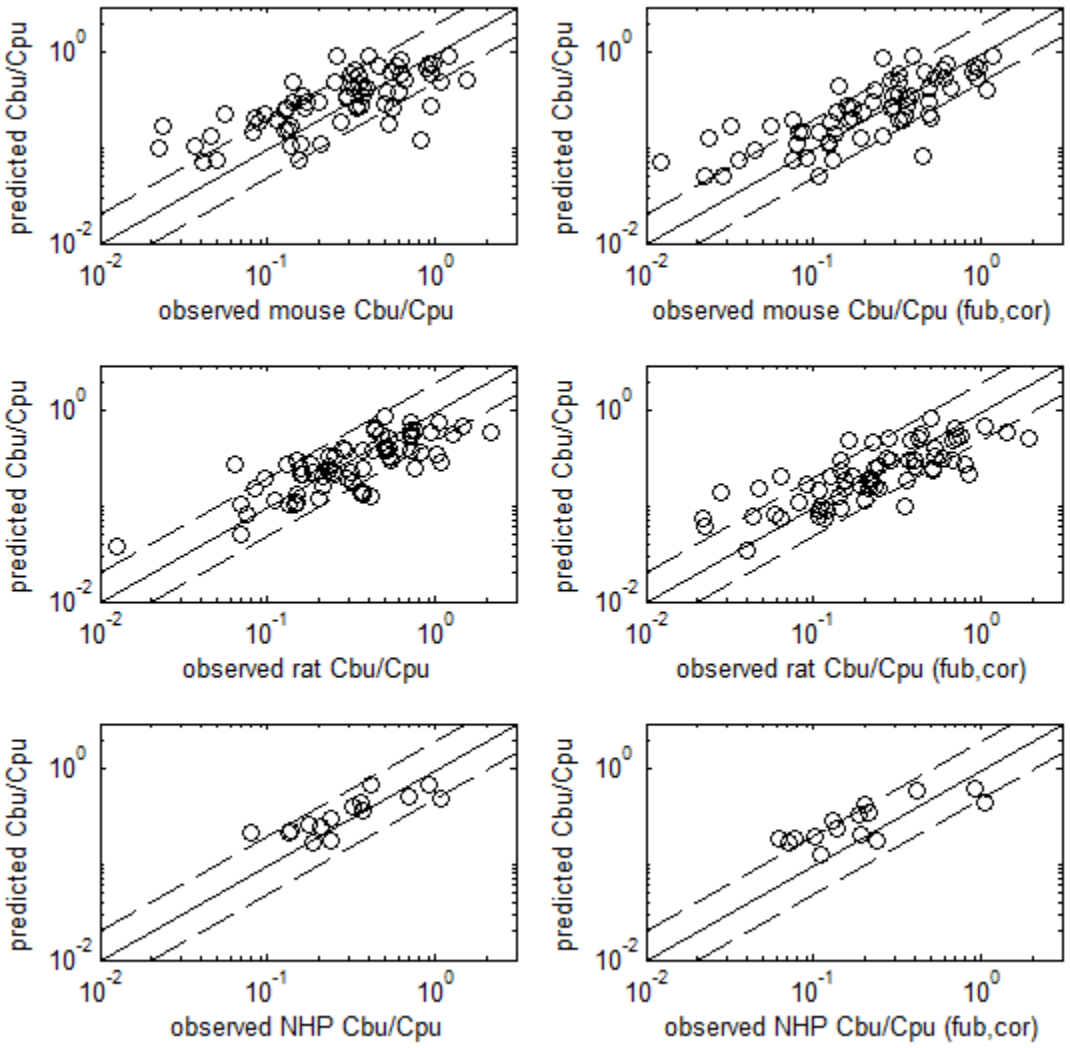

DMD Fast Forward. Published on January 25, 2019 as DOI: 10.1124/dmd.118.083279
This article has not been copyedited and formatted. The final version may differ from this version.

Figure 4.

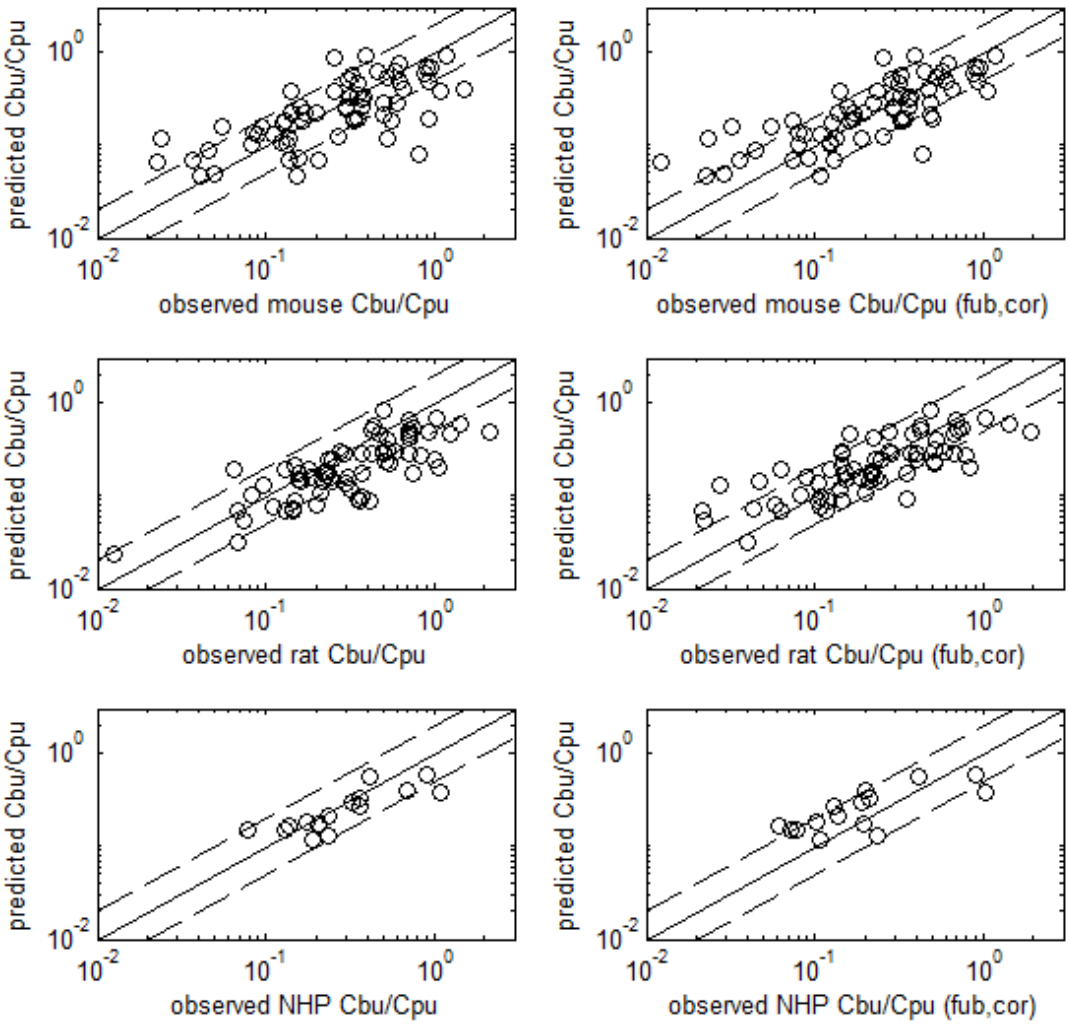

DMD Fast Forward. Published on January 25, 2019 as DOI: 10.1124/dmd.118.083279
This article has not been copyedited and formatted. The final version may differ from this version.

Figure 5.

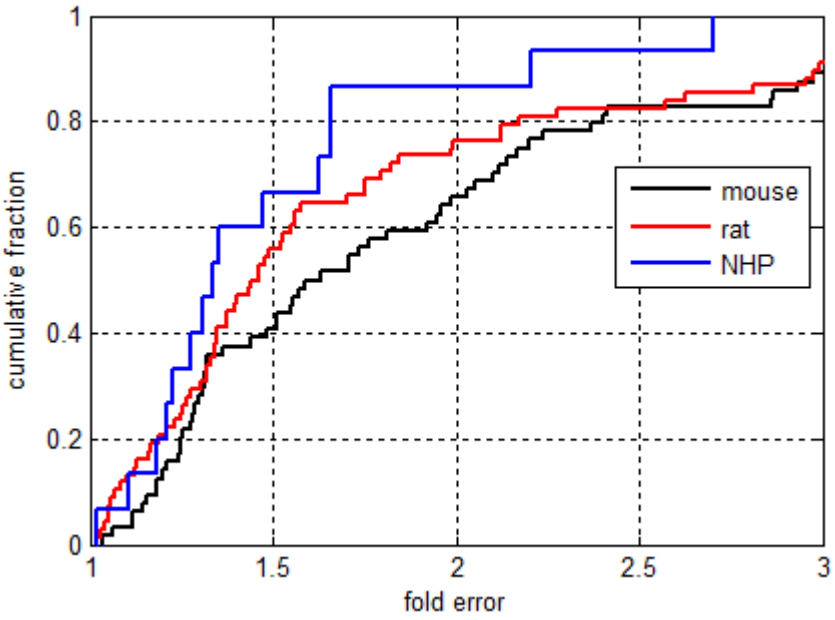

DMD Fast Forward. Published on January 25, 2019 as DOI: 10.1124/dmd.118.083279
This article has not been copyedited and formatted. The final version may differ from this version.

Figure 6.

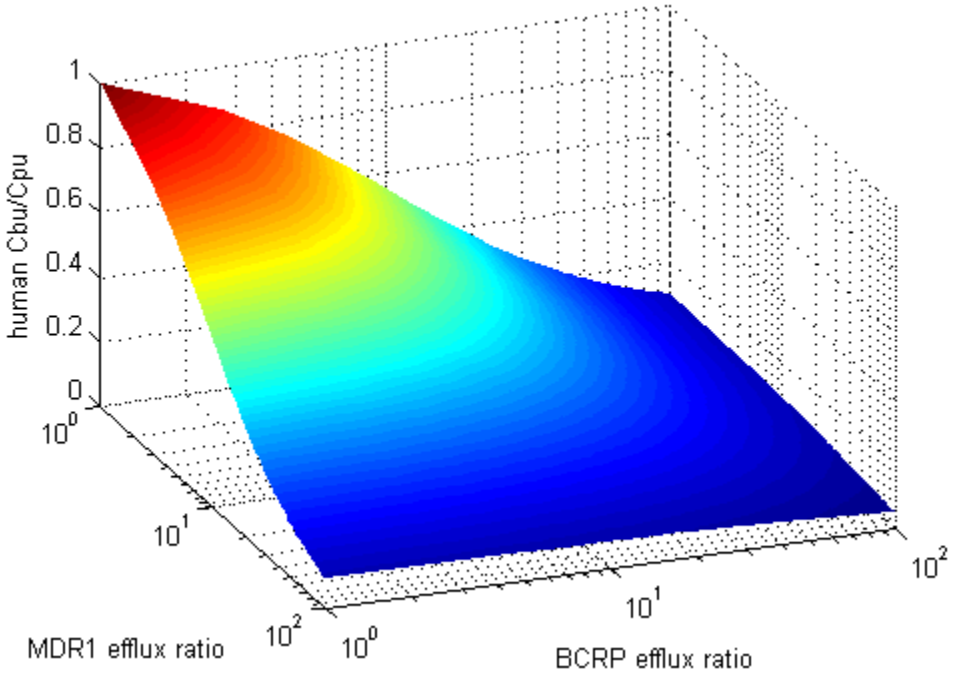

DMD Fast Forward. Published on January 25, 2019 as DOI: 10.1124/dmd.118.083279
This article has not been copyedited and formatted. The final version may differ from this version.

Figure 7.